공학석사학위논문

Fabrication of Highly Porous Polyaniline/Carbon Nanodots for Efficient Counter Electrodes in Dye-sensitized Solar Cells

염료감응형 태양전지의 효율적인 상대전극을 위한 다공성 폴리아닐린/탄소나노점 나노복합재의 제조

2016년 2월

서울대학교 대학원

화학생물공학부

이 기 수

Abstract

Fabrication of Highly Porous Polyaniline/Carbon Nanodots for Efficient Counter Electrodes in Dye-sensitized Solar Cells

Kisu Lee

School of Chemical and Biological Engineering

The Graduate School

Seoul National University

We synthesized highly porous polyaniline (PANI) using carbon nanodots (CNDs) as a nucleating agent and demonstrate their use as counter electrodes (CEs) for dye-sensitized solar cells (DSSCs). CNDs surrounded with aniline

act as efficient nuclei of the polymerization reaction. CNDs disrupt undesirable second growth reactions leading to agglomerated structure, and organize the highly porous PANI structures with a large surface area (43.6 m^2g^{-1}). Moreover, the presence of CNDs in the polymerization mixture facilitates generation of head-to-tail dimers, and enhances the degree of *para*-coupling in molecular structure of PANI. As a result of these nucleation effects, fabricated PANI-CND films exhibit increased electrical conductivity of *ca.* 774 S cm^{-1}. When used as a CE in DSSCs, PANI-CND CEs exhibit superior power conversion efficiencies (η= 7.45%) than those of conventional platinum (η= 7.37%) and pristine PANI CEs (η= 5.60%).

Keyword: Polyaniline, Carbon nanodots, Self-stabilized dispersion polymerization, Dye-sensitized solar cells, Counter electrodes.

Student number: 2014-20627

List of Abbreviations

DSSC: Dye-sensitized Solar Cell

CE: Counter Electrode

PCE: Power Conversion Efficiency

PANI: Polyaniline

SSDP: Self-stabilized Dispersion Polymerization

CSA: Camphorsulfonic Acid

CND: Carbon Nanodot

APS: Ammonium Persulfate

ES: Emeraldine Salt

EB: Emeraldine Base

FTO: Fluorine-doped Tin Oxide

TEM: Transmission Electron Microscope

HR-TEM: High Resolution Transmission Electron Microscope

XPS: X-ray Photoelectron Spectroscopy

PL: Photoluminescence

FE-SEM: Field-emission Scanning Electron Microscope

BET: Brunauer-Emmett-Teller

BJH: Barrett-Joyner-Halenda

FTIR: Fourier-transform Infrared

NMR: Nuclear Magnetic Resonance

AFM: Atomic Force Microscope

XRD: X-ray Diffraction Spectroscopy

CV: Cyclic Voltammetry

EIS: Electrochemical Impedance Spectroscopy

R_a: Surface Roughness

R_s: Series Resistance

R_{ct}: Charge Transfer Resistance

E_{pp}: Peak-to-peak Voltage Separation

V_{oc}: Open-circuit Voltage

J_{sc}: Short-circuit Current Density

FF: Fill Factor

List of Figures

Figure 7. (a) Electrical conductivity of PANI and PANI-CND films with different CNDs concentrations. (b) X-ray diffraction patterns of the films in (a).

Figure 8. Cross-sectional SEM images of (a) PANI and PANI-CND films with different CNDs concentrations: (b) 1, (c) 5, and (d) 10 wt%.

Figure 9. (a) CV curves of Pt, PANI and PANI-CND on FTO substrates in I^{3-}/I^{-} electrolyte composed of 10 mM LiI, 1 mM I_2, and 0.1 M $LiClO_4$ in acetonitrile at a scan rate of 50 mV s^{-1}. (b) Nyquist plots of symmetrical dummy cells employing Pt, PANI and PANI-CND counter electrodes (CEs). The frequency scan range was set from 0.1 Hz to 1 MHz with amplitude of 10 mV. Inset is the equivalent circuit. (c) Tafel polarization curves measured for the same devices used in the EIS measurements at a scan rate of 50 mV s^{-1}. PANI-CND CE for the measurements was fabricated with PANI-CND (5 wt%).

Figure 10. AFM images and cross-sectional analyses (1 X 1 μm^2 scale) of (a) PANI and (b) PANI-CND counter electrodes (CEs). Measured surface roughness (R_a) values of the samples are 0.39 and 0.67 nm, respectively. PANI-CND CE was fabricated with PANI-CND (5 wt%).

Figure 11. *J–V* characteristics of DSSCs with Pt, PANI and PANI-CND counter electrodes (CEs) and inset is a photograph of electrodes made with Pt and PANI-CND (top) and assembled DSSCs with the each CEs (bottom). PANI-CND CE for the measurements was fabricated with PANI-CND (5 wt%).

Figure 12. *J-V* characteristics of DSSCs employing PANI and PANI-CND counter electrodes with different CNDs concentrations: 1, 5, and 10 wt%.

List of Tables

Contents

Chapter 1. Introduction

1.1 Counter electrodes in DSSCs

In dye-sensitized solar cell (DSSC) systems, platinum (Pt)-based counter electrode (CE) is one of the major hurdles for large-scale production of DSSCs owing to high cost and scarce resource of Pt [1,2]. For this reason, alternative CE materials with low cost, high chemical stability, and high electro-catalytic activity are highly desirable. Recently, various CEs based on carbon materials, transition metal complexes, and conducting polymers have been investigated as promising candidates to replace Pt-based CE [3]. Especially, conducting polymers have many merits of high electrochemical activity, transparency, low cost, and simple preparation [4-6].

1.2 Polyaniline-camphorsulfonic acid (PANI-CSA)

As a representative conducting polymer, polyaniline (PANI) is suitable for CEs because of its superior catalytic activity for I_3^- reduction and environmental stability [7,8]. Among the various preparation methods of PANI electrodes, PANI-camphorsulfonic acid (CSA) can produce PANI thin-films with two or three orders of magnitude higher electrical conductivity ($\geq$ 500 S cm^{-1}) than that of pristine PANI powder due to expanded chain conformation with the help of CSA and *meta*-cresol solvent [9-11]. Several studies utilized PANI-CSA for CEs in DSSCs, and represented conversion efficiencies of 5.5 %, 6.2 %, and 6.3 % [12-14]. However, the still insufficient conductivity has limited the high conversion efficiency of DSSCs with PANI-CSA electrodes. One of the main reasons to degrade electrical properties of PANI-CSA film is the low surface area of PANI before solvation with *meta*-cresol. Typically, PANI is polymerized at low temperature to achieve high purity in molecular structure [15]. This method requires long reaction time to attain a sufficient yield ($\geq$ 30%) of PANI. During this time, polymer structures agglomerate by the growth onto the previously formed polymer, known as the secondary growth [16]. The agglomerated structure leads to a lower surface area that is available for contact with the doping agent or solvent, eventually resulting in deteriorated

electrical properties of PANI-CSA films. Therefore, organizing nanostructured PANI without agglomeration during the entire polymerization process is crucial to the electrochemical performance of PANI-CSA electrodes as CEs in DSSCs.

1.3 Carbon nanodots (CNDs)

Carbon nanodots (CNDs) are carbonaceous clusters of less than 10 nm in diameter, which have received growing interests as a state of the art nanomaterial due to their ease of synthesis, chemical inertness, and low toxicity [17-19]. Despite recent improvements in the synthesis and application of CNDs, however, the effects of CNDs on the structural, electrical, and electrochemical properties of conducting polymers have not been widely reported. In this work, CNDs played an important role in organizing porous structures of PANI by providing the nuclei of polymerization to prevent the secondary growth. The surface state of CNDs with rich carboxyl groups is appropriate for combination with aniline monomers and nanometer-sized dots could function as an efficient nucleating agent even at a low concentration.

1.4 Objective of this study

Herein, we report a novel method to synthesize highly porous nanostructured PANI using CNDs as a nucleating agent for high-performance CEs of DSSCs. The nucleation effects of the CNDs on the structural and electrical characteristics of PANI-CND nanocomposites were systematically investigated by nitrogen adsorption/desorption isotherms, FT-IR, NMR spectroscopies, and XRD patterns, respectively. The CEs made with PANI-CND exhibited excellent electro-catalytic activity comparable to conventional Pt-based CEs and were characterized using CV and EIS measurements. The results show that zero-dimensional carbon materials can have great impacts on the structural and electrical properties of PANI. To the best of our knowledge, this is the first demonstration of using CNDs to enhance electrochemical performance of PANI-CSA as a CE of DSSC.

Chapter 2. Experimental

2.1 Materials

Citric acid (99%), aniline (99%), and ammonium persulfate (APS, 98%) were obtained from Sigma-Aldrich (St. Louis, MO,USA). TiO_2 nanoparticles (Ti-nanoxide T/SP), cis-disothiocyanato-bis(2,20-bipyridyl-4,40-dicarboxylato)ruthenium-(II)bis-(tetrabutylammonium) (N719), butylmethylimidazolium iodide, lithium iodide, and iodine were purchased from Solaronix (Aubonne, Switzerland). Hydrochloric acid (HCl, 35–37%), boric acid (H_3BO_3, 99.5%), chloroform ($CHCl_3$, 98%) and ammonia solution (NH_4OH) were purchased from Samchun (Seoul, Korea).

2.2 Preparation of CNDs

1 g of citric acid was transferred into a Teflon-lined autoclave (20 mL) and then heated at 180 °C in an electric oven for 4 h. In order to neutralize the CNDs, NaOH aqueous solution (10 mg/mL) was dropped into the resulting orange transparent liquid. The CND powder could be obtained by adding ethanol solvents into the CNDs solution followed by the

centrifugation at 10,000 rpm for 10 min. The precipitates of CNDs were dried in an oven at 60 °C.

2.3 Synthesis of PANI-CND nanocomposite

PANI-CND emeraldine salt (ES) powder was synthesized using a self-stabilized dispersion polymerization (SSDP) method based on chemical oxidation polymerization at −42.5 °C [15]. 2 g of aniline monomer and 10 mL of HCl solution were added to 30 mL of deionized water. The obtained CND powder (the weight percentage of CND powder were 1 wt%, 5 wt%, 10 wt% with respect to aniline, respectively) and boric acid (1 mg) were dispersed into the aqueous anilinium ion solution, and then the solution was stirred at 50 °C for 3 h to passivate. 60 mL of chloroform was poured into the aqueous anilinium ion solution in order to induce interfacial polymerizations of aniline monomers. Oxidizing agent was prepared by adding 2.4g of APS and 6 mL of HCl into the 10 mL of deionized water, and the resulting oxidizing agent was added into the reaction medium to initiate polymerization at –9 °C. The polymerization of aniline proceeded with vigorous stirring for 16 h at –42.5 °C. After washing with water, ethanol, and acetone, precipitates of greenish PANI-CND ES powder were obtained.

2.4 Fabrication of the PANI-CND nanocomposite film

The PANI-CND ES was fully reduced by adding 207.5 mL of 0.6 M NH_4OH solution as a reducing agent. The products were washed with water, ethanol, and acetone as above in order to gain brownish PANI-CND emeraldine base (EB) powders. Secondary doping of the PANI-CND EB powders was conducted with CSA (CSA : PANI-CND EB = 2 : 1 by mole). 0.165 g of CSA-doped PANI-CND powders were dissolved in 5.0 mL of *meta*-cresol/chloroform (7:3, v/v) co-solvent. The solution was vigorously stirred and sonochemically treated for 24 h to increase the solubility of PANI-CND powders within the solutions. In order to prepare PANI-CND films, the resulting CSA-doped PANI-CND solutions were fabricated as thin films onto fluorine doped tin oxide (FTO) substrate using a spin-coater at 5000 rpm for 30 s. The spin-coated thin films were dried at 40 °C for 16 h, and finally 650 nm PANI-CND films on FTO substrates were obtained.

2.5 Assembly of DSSC with PANI-CND counter electrode

FTO glass substrates were washed with deionized water, acetone and 2-propanol for 60 min, respectively. The FTO glass substrate for photoanode were pretreated with 40 mM $TiCl_4$ aqueous solution and heated at 450 °C for

30 min to form TiO_2 compact layers onto the FTO substrates. A paste of TiO_2 nanoparticles was screen-printed onto the FTO glass substrate. Sintering of the TiO_2-coated FTO glasses was carried out at 450°C for 30 min. The FTO glasses with TiO_2 thin films were immersed in the dye solution (0.5mM N719 dye in absolute ethanol) for 18 h at 25 °C. As-prepared working electrodes were assembled with the PANI-CND films on FTO substrates into sandwich-type cells. A drop of the redox electrolyte (0.6 M butylmethylimidazolium iodide , 0.1 M LiI, and 0.5 M tert-butylpyridine in acetonitrile) was injected into the cell. For comparison of the overall performance to conventional CE, a Pt-coated CE was prepared by dropping 5 mM chloroplatinic acid hexahydrate ($H_2PtCl_6 \cdot 6H_2O$) onto the FTO substrate followed by heating treatment at 400°C for 30 min.

2.6 Characterization of materials and DSSC performance

Transmission electron microscope (TEM) and high resolution transmission electron microscope images were obtained with JEM 2100 and JEM 3010 (JEOL, Japan). Morphological images of PANI-CND were acquired using a field-emission scanning electron microscope (FE-SEM, JSM-6701F, JEOL, Japan) and an atomic force micrscope (AFM) (Innova

SPM, Vecco, USA). The X-ray photoelectron spectra (XPS) were recorded by AXIS-His spectrometer (Kratos/Shimadzu, Kyoto, Japan). Brunauer–Emmett–Teller (BET) surface areas and Barret-Joyner-Halenda (BJH) pore size distributions of PANI were obtained using Micromeritic analyzer (ASAP 2000, Micromeritic Co., USA). Microstructural characterizations of PANI-CND EB were investigated by the Fourier-transform infrared (FTIR) spectra (Frontier FT-IR spectrometer, Perkin Elmer, USA) and solid state ^{13}C NMR spectra (Avance Ⅱ, Bruker, Germany). The electrical conductivity was measured with the four-probe system using a KEITHLY 2400 (KEITHLY, USA). The X-ray diffraction (XRD) patterns were taken by Smartlab (Rigaku, Japan). CV (WBCS 3000, Wonatech, Korea) was conducted in an electrolyte containing 10 mM LiI, 1 mM I_2, and 0.1 M $LiClO_4$ in acetonitrile. The symmetrical dummy cells were prepared by assembling two identical CEs and injecting the electrolyte as used for DSSC to measure EIS and Tafel polarization curves using Zive lab (Wonatech, Korea). The photocurrent-voltage (I-V) characteristics of DSSCs with various CEs were evaluated using a 500 W xenon lamp (XIL model 05A50KS source units; AM 1.5G solar irradiance; intensity: 100 mW cm^{-2}).

Chapter 3. Results and discussion

3.1 Synthesis of the PANI-CND nanocomposite

Figure 1 illustrates the overall procedure to synthesize highly porous PANI using CNDs as a nucleating agent and obtain PANI-CND electrodes. CNDs were prepared using a solvothermal process from citric acid. TEM and HR-TEM images of CNDs are shown in Figure 2a. The mean diameter of the as-made nanodots was *ca.* 4.1 nm, with a narrow size distribution of ±0.6 nm. The inset image suggests that the interior of the CNDs has a lattice spacing of 0.24 nm, corresponding to the (1120) face of graphite [20,21]. Conversely, XPS spectra in Figure 2b indicate that the surface of the CNDs has rich oxygen-containing functional groups. In particular, A peak of 288.6 eV related to carboxyl groups is predominant, which are favorable for reaction with aniline. The obtained CNDs combined with anilinium ions by boric acid which catalyzes formation of amide bonds between carboxyl groups and amine groups [22,23]. Photoluminescence (PL) and zeta potential measurements were conducted to identify transition in the surface states of CNDs by combination with aniline monomers (Figure 3). PL spectra of CNDs red-shifted after passivation because the amine groups of aniline

lower the band gap of CNDs by donating electrons [24]. The zeta potentials of CNDs and passivated CNDs were determined to be −15.2 mV and −5.4 mV, respectively. The negatively charged CNDs were partially neutralized by interaction with aniline monomers [25]. After combination of CNDs with aniline monomers, anilinium ions preferentially arranged themselves around the surfaces of CNDs passivated with benzene rings. As an ammonium persulfate (APS) solution was added to produce radicals, CNDs aggregated with aniline monomers began to precipitate due to the insolubility of PANI in water. These precipitates acted as nucleation points, grew to polymer, and resulted in highly defined porous PANI. The obtained PANI-CND was subsequently dedoped with ammonium hydroxide and given a secondary doping with CSA. This was then dissolved in *meta*-cresol/chloroform solvents, spin-coated onto substrates, and annealed to yield transparent green PANI-CND electrodes.

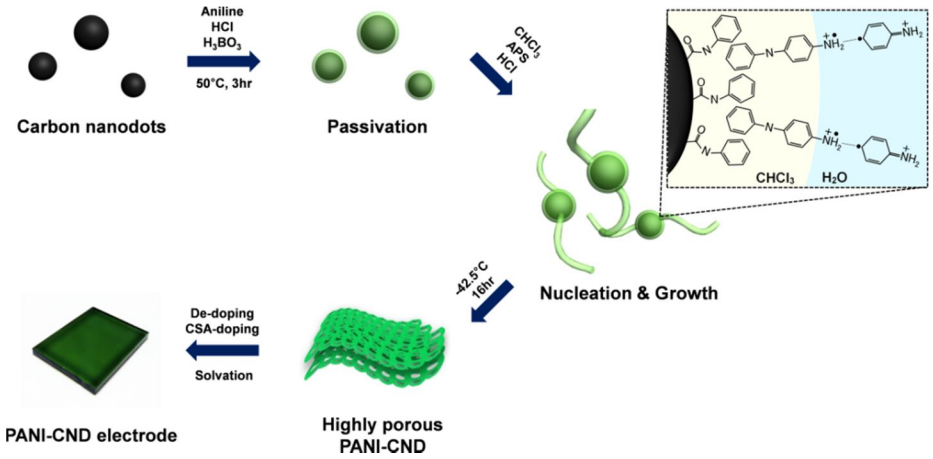

Figure 1. A schematic illustration showing synthesis of PANI-CND nanocomposite and fabrication of the PANI-CND nanocomposite film.

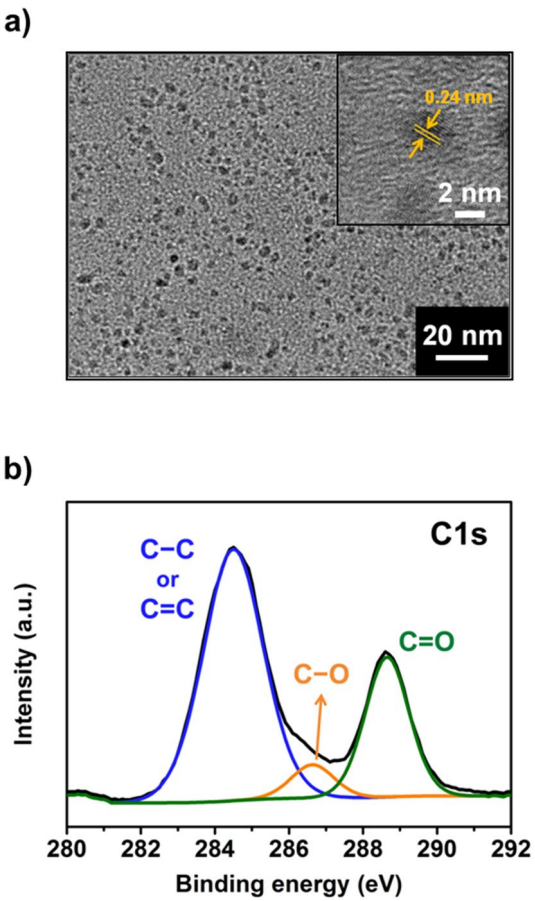

Figure 2. (a) A TEM image of CNDs obtained from citric acid using solvothermal synthesis. Inset shows a HR-TEM image of CNDs. (b) C (1s) peaks in the XPS spectrum of CNDs.

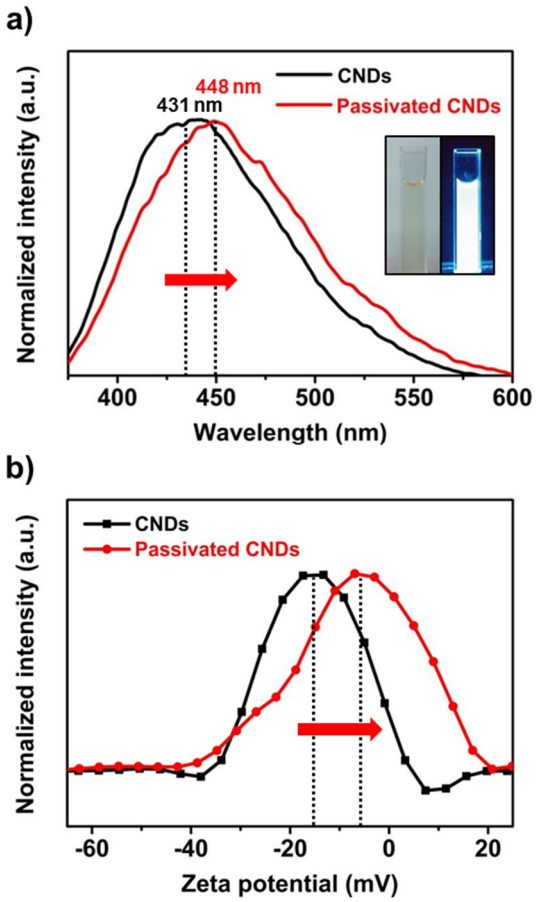

Figure 3. (a) Photoluminescence spectra of CNDs and passivated CNDs under 350 nm excitation and inset is photographs of photoluminescent CNDs. (b) Zeta potential graphs for CNDs and passivated CNDs.

3.2 Characterization of the PANI-CND nanocomposite

3.2.1 Highly porous morphology

In FE-SEM images of Figure 4, the morphological features of PANI are observed by varying the concentrations of CNDs added into the polymerization mixture. The micrograph of Figure 4a shows pristine PANI after polymerization. Secondary growth on previously formed structures was evident and the original porous structure was obscured by agglomeration. In contrast, PANI that had been formed *via* nucleation on CNDs exhibited a highly defined and porous structure. The CNDs facilitated the continuous generation of nuclei such that homogeneous nucleation was maintained despite relatively long polymerization times. In general, newly polymerized PANI molecules could either grow from previously constructed PANI structures (heterogeneous nucleation) or from nuclei (homogeneous nucleation) [16]. In conventional methods, heterogeneous nucleation is preferred in the later stages of polymerization because PANI structures that are already formed become dominant [16]. On the other hand, nuclei generated from CNDs can easily exceed supersaturation levels, thereby facilitating homogeneous nucleation even during the later stages of polymerization. Thus, in the presence of CNDs, agglomerated structure

resulting from secondary growth were prevented and the high-surface-area porous structure that characterizes the initial stage of polymerization was preserved. However, when adding CNDs more than the optimized amount (5 wt%), PANI structure agglomerated because excessive nuclei generated from CNDs might aggregate among themeselves (Figure 4d).

The porosity of PANI and PANI-CND was determined by measuring nitrogen adsorption and desorption isotherms (Figure 5a). The curves of both materials exhibited hysteresis when the nitrogen was desorbed, indicating that the samples were mesoporous materials [26-28]. Surface areas and total pore volumes were obtained using the BET method (Table 1). Among the samples, PANI with 5 wt% CNDs had the largest surface area of 43.64 $m^2 g^{-1}$, which was 3.5 times that of pristine PANI (12.43 $m^2 g^{-1}$). Both surface area and pore volume decreased at CND weight ratios exceeding 5%, indicating that excessive nucleation caused agglomeration as shown in Figure 4d. Figure 5b shows the size distribution of pores in the PANI structure. No obvious peaks were observed in the pore size distribution of pristine PANI on account of its agglomerated morphology, but the number of pores in PANI-CND ranging from 20 to 50 nm significantly increased.

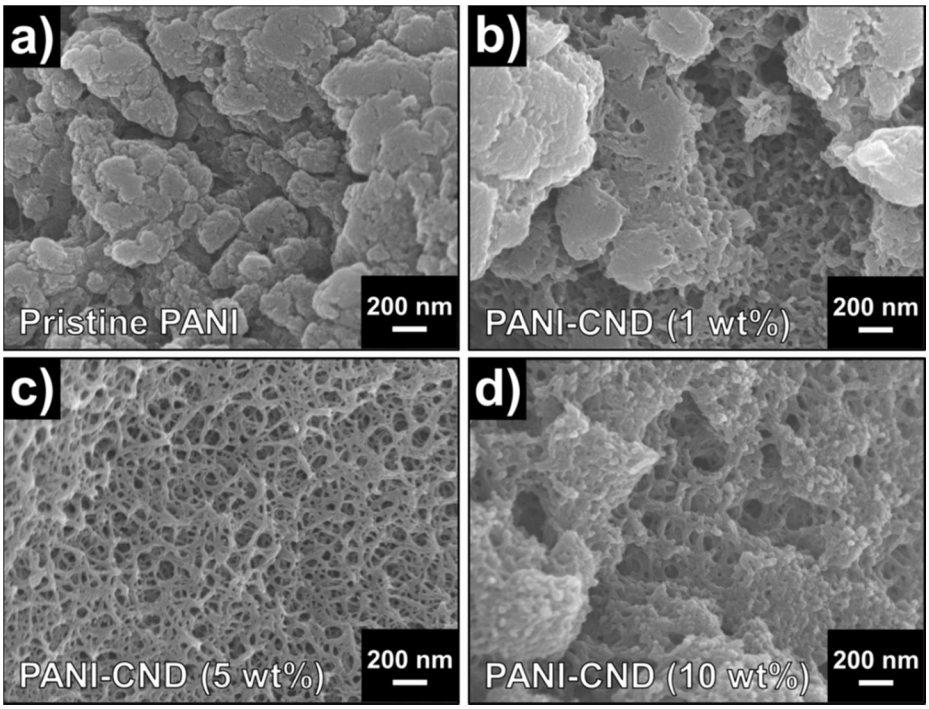

Figure 4. (a) FE-SEM images of synthesized (a) PANI and PANI polymerized with the addition of (b) 1 wt%, (c) 5 wt%, and (d) 10 wt% of CNDs. All the polymerization reactions proceeded for 16 h after the initiator solution was added into the aqueous anilinium solution.

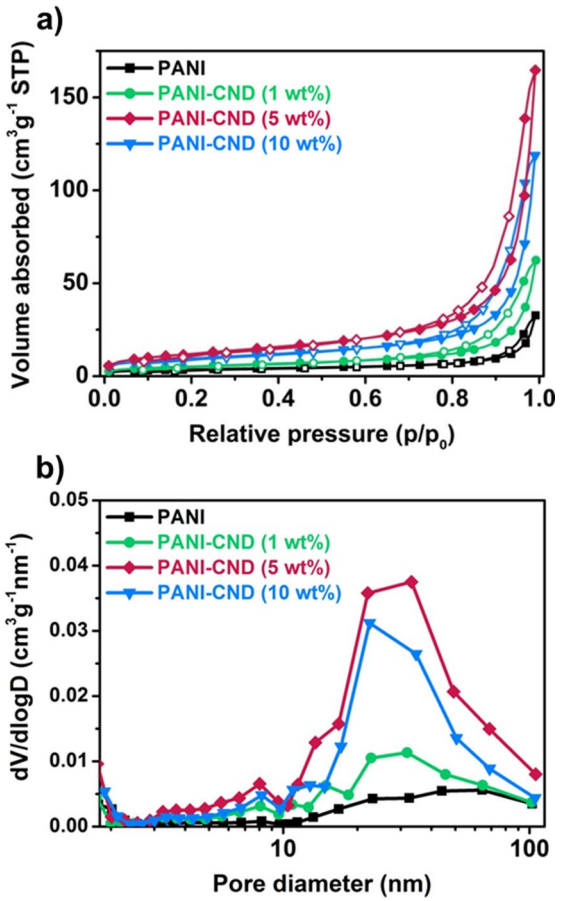

Figure 5. (a) Nitrogen adsorption (solid symbol)/desorption (hollow symbol) isotherms and (b) Barret-Joyner-Halenda (BJH) pore size distribution of PANI and PANI-CND with different CNDs concentrations.

Table 1. Brunauer–Emmett–Teller (BET) surface areas and total pore volumes of PANI and PANI-CND.

Sample	Surface area ($m^2 g^{-1}$)	Total pore volume ($cm^3 g^{-1}$)
PANI	12.43	0.051
PANI-CND (1 wt%)	18.79	0.096
PANI-CND (5 wt%)	43.64	0.255
PANI-CND (10 wt%)	34.04	0.184

3.2.2 Molecular structure

The nucleation of PANI on CNDs not only constructed porous morphology of the polymer, but also improved purity of PANI molecular structure. To compare the as-prepared samples with their ideal molecular structures, PANI and PANI-CND emeraldine base (EB) were characterized by FT-IR and ^{13}C NMR spectroscopies. The degree of *para*-coupling in the PANI microstructure was estimated from FT-IR spectra (Figure 6a). The absorption band at *ca*. 1500 cm^{-1} is attributable to the C=C stretching vibration mode of the benzene ring [15]. This peak is infrared-inactive when the benzene moiety is substituted with identical groups on a *para*-pair [15]. The absorption band at 820 cm^{-1} originates from the C–H out-of-plane bending mode of the 1,4-disubstituted benzene ring [15]. Thus, a ratio of peak intensities at 820 cm^{-1} and 1500 cm^{-1} (I_{820}/I_{1500}) was used to measure the degree of *para*-coupling in PANI. The I_{820}/I_{1500} ratio of PANI-CND (I_{820}/I_{1500} = 0.94) increased by 0.13 with respect to that of pristine PANI (I_{820}/I_{1500} = 0.81), indicating an enhancement in the degree of *para*-coupling. The ^{13}C NMR spectra in Figure 6b, obtained using the CP MAS method, indicated an alternating benzenoid–quinoid structure in the PANI EB [15]. Three individual peaks and three shoulder peaks were observed at 113 (shoulder), 122, 137 (shoulder), 141, 148 (shoulder), and 157 ppm, relative

to the tetramethylsilane, in the NMR spectra of samples. These peaks were assigned to carbon atoms in ideal molecular structure of the PANI EB. In particular, the peak at 137 ppm corresponds to protonated carbon atom C4 in quinoid ring owing to the inability to rotate around the bent linkage of the imine group (=N-) in the idealized repeat unit of the PANI EB [29]. The peak at 137 ppm in the spectra of PANI-CND increased relative to that of pristine PANI, implying that the alternating microstructure in the *para*-direction was enhanced. These enhancement in the degree of *para*-coupling resulted from the nucleation on CNDs, which significantly decreased generation of undesirable dimers by facilitating the head-to-tail coupling. In general, three types of dimer can be formed upon the oxidation of aniline *via* 1) head-to-tail coupling (*para*-aminodiphenylamine), 2) head-to-head coupling (*N*,*N*-diphenylhydrazine), or 3) tail-to-tail coupling (benzidine) [30,31]. Two dimeric species of *N*,*N*-diphenylhydrazine and benzidine may also participate in the propagation of the polymer chain, but these dimers reduce the degree of *para*-coupling [30,31]. In our method, aniline monomers assumed a specific orientation due to the hydrophobicity of the passivated CNDs, resulting in more head-to-tail coupling. By facilitating the generation of desirable dimers, ideal PANI microstructures were realized with high purity.

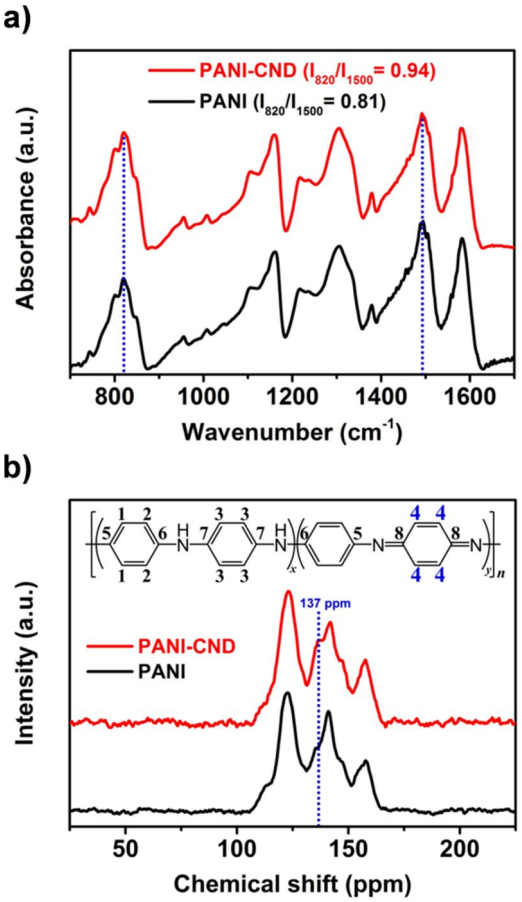

Figure 6. (a) FT-IR spectra and (b) solid state ^{13}C NMR spectra of PANI and PANI-CND (5 wt%) emeraldine base obtained by deprotonating emeraldine salt powder.

3.3 Electrical conductivity and crystallinity of the PANI-CND nanocomposite film

The effect of CND-induced nucleation on the electrical conductivity and crystalline structure of CSA-doped PANI films were determined using four-point probe resistivity measurements and XRD studies. Figure 7a shows the electrical conductivity of PANI and PANI-CND films. The maximum film conductivity (815 S cm^{-1}, average: 774 S cm^{-1}) of PANI-CND was obtained with 5 wt% CNDs. The average conductivity of the pristine PANI films was *ca*. 596 S cm^{-1}. This increase in conductivity can be explained as follows. 1) The increased surface area of PANI-CND facilitated dedoping and secondary doping reactions. The highly defined porous structure of PANI-CND can be more effectively reduced with NH_3 molecules and can accommodate more CSA molecules during secondary doping, relative to PANI synthesized by conventional means. 2) Interactions between the PANI and *meta*-cresol/chloroform solvents may be increased due to the enlarged surface area of PANI-CND. It is known that the *meta*-cresol/chloroform solvents induce the electrostatic repulsion between positive charges on the PANI chains [32]. Hence, the highly porous PANI-CND structure resulted in more expanded coil conformation and higher linearity of the polymer chains, which greatly enhanced the crystallinity of the PANI-CND films. For this

reason, cross sections of drop-casted PANI and PANI-CND films clearly showed a different stacked morphology. In FE-SEM images of Figure 8, PANI-CND (5 and 10 wt%) films are densely stacked with vertical separation relative to pristine PANI and PANI-CND (1 wt%) films. Relatively larger surface areas of PANI-CND (5 and 10 wt%) strengthened stacking of polymer chain along the particular direction and increased the crystalline phase of the films [32]. 3) Nucleation on CNDs enhanced the conjugation length of the PANI polymer backbone by improving the quality of molecular structure as evidenced by FT-IR and ^{13}C NMR data. XRD patterns of the prepared films are shown in Figure 7b. Three major peaks of the patterns were observed at 15°, 20°, and 25°. When the sample became more metallic, the peak at 25°, which corresponds to the degree of interchain stacking between the phenyl rings of PANI, increased and sharpened [33,34]. The peak intensity at 25° dominated the pattern after the addition of the CNDs, indicating an enhancement in the interchain stacking and π-conjugation length of the PANI.

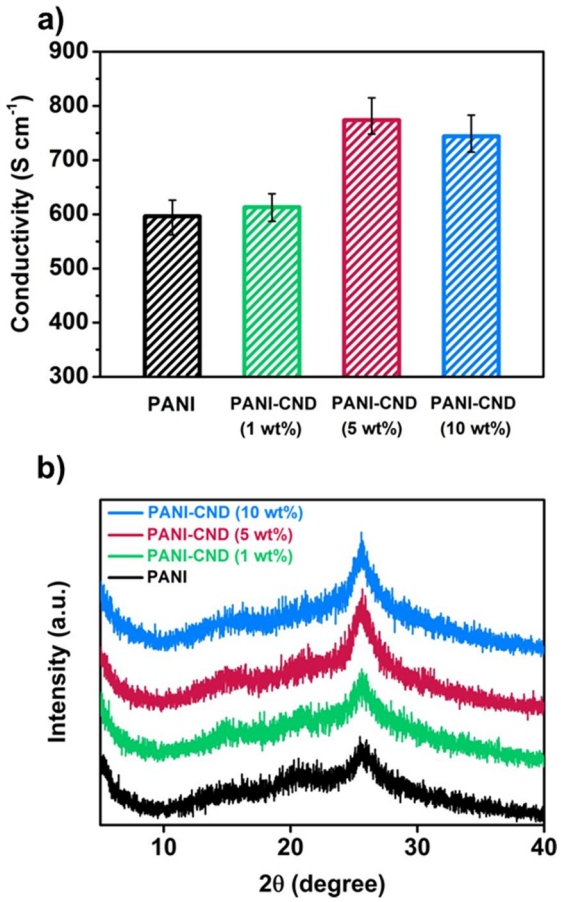

Figure 7. (a) Electrical conductivity of PANI and PANI-CND films with different CNDs concentrations. (b) X-ray diffraction patterns of the films in (a).

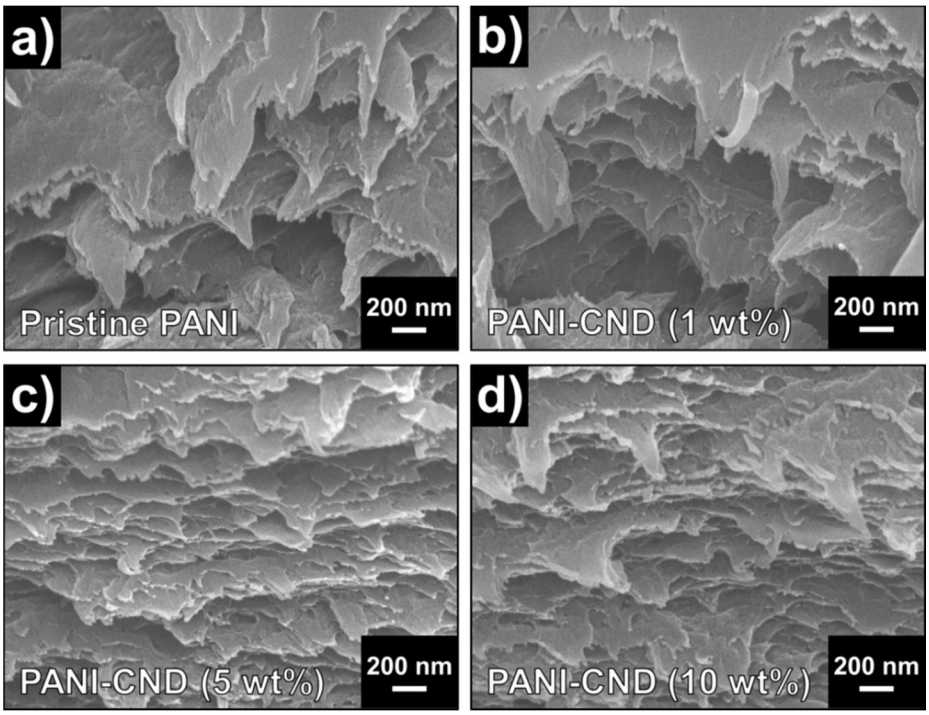

Figure 8. Cross-sectional SEM images of (a) PANI and PANI-CND films with different CNDs concentrations: (b) 1, (c) 5, and (d) 10 wt%.

3.4 PANI-CND counter electrode in DSSC

3.4.1 Electrochemical performance of PANI-CND CE

To evaluate the electro-catalytic activity of the fabricated PANI-CND CE against that of conventional CEs based on Pt or PANI, cyclic voltammetry (CV) was performed using a three-electrode system and the I_3^- /I^- redox pair. The CVs in Figure 9a show typical I_3^-/I^- redox peaks obtained on Pt, PANI, and PANI-CND CEs. The cathodic peaks of I_3^-/I^- on PANI and PANI-CND CEs appeared at –0.24 V and –0.14 V, respectively. These peaks represent the reduction of I_3^- to I^-, which is the main function of CEs [35]. The anodic peaks on PANI and PANI-CND CEs occurred at 0.60 V and 0.55 V, corresponding to the oxidation of I^- to I_3^- [35]. The current densities at the cathodic peaks, which are used to evaluate electro-catalytic activity of CEs, obtained on PANI and PANI-CND CEs were –6.18 mA cm^{-2} and –7.66 mA cm^{-2}, respectively. In addition, the PANI-CND CE exhibited better peak-to-peak voltage separation (E_{pp}) compared to that of the PANI CE. The E_{pp} of the PANI-CND CE was 0.69 V, while that of the PANI CE was 0.84 V. The improvements in the peak current densities and the E_{pp} of PANI-CND electrode indicate enhancement in the catalytic activity to facilitate the triiodide regeneration, which were attributable to the enhanced electrical

conductivity [35,36]. But besides electrical conductivity, active surface area of CEs for interaction with I_3^-/I^- redox can also impact on electro-catalytic activity, so surface roughness of film-type CEs is directly related to the conversion efficiency of DSSC [37]. We observed surface morphology of the PANI and PANI-CND CEs using an atomic force microscope (AFM) (Figure 10). Measured surface roughness (R_a) values are presented together. Surfaces of spin-coated PANI and PANI-CND CEs from the viscous solution are extremely flat. However, the surface of PANI-CND CE seemed to be rougher than that of pristine PANI CE in cross-sectional analysises. Moreover, R_a of PANI-CND CE (0.67 nm) was larger than that of pristine PANI CE (0.39 nm). CNDs might affect organization of the grains in spin-coated PANI films, cause a rough surface, and increase catalytic sites for I_3^- reduction. Increased electrical conductivity and surface roughness made a synergy effect, eventually enhancing electro-catalytic activity of PANI-CND CE. Electrochemical impedance spectroscopy (EIS) was conducted to further clarify the electron transport at the PANI-CND CE interface in symmetrical dummy cells. The resulting Nyquist plots are presented in Figure 9b. Series resistance (R_s) and charge transfer resistance (R_{ct}) values are listed in Table 2. These parameters were calculated by fitting the EIS spectra in accordance with the Randle's circuit shown in Figure 9b. The intercept on the real axis in the high frequency domain determines R_s, which represents the interfacial resistance of ohmic contact between the CE and the FTO substrate [38,39].

The R_s of PANI and PANI-CND CEs were almost identical (13.15 Ω cm^{-2}, 13.19 Ω cm^{-2}) and were much lower than that of the Pt CE (17.89 Ω cm^{-2}). These results indicate that both the PANI-CND and PANI CE are very compatible with FTO substrates due to the high polarity of the *meta*-cresol solvent [32]. R_{ct}, the resistance between the CE and the I_3^-/I^- electrolyte, was determined by measuring the arc of the left semicircle in the Nyquist plot [38,39]. The R_{ct} of the PANI-CND CE (2.93 Ω cm^{-2}) was significantly lower than that of the PANI CE (12.77 Ω cm^{-2}) due to its enhanced electro-catalytic activity resulting from the synergy effect of increased electrical conductivity and surface roughness [3]. In addition, R_{ct} is directly related to the exchange current density ($J_0 = RT/nFR_{ct}$), which can be estimated from the extrapolated intercepts of the cathodic branches on the left side of the Tafel polarization curves shown in Figure 9c [40]. Among the three samples, the Pt CE exhibited the highest slope for the cathodic branch and exchange current density. However, the analogous slope of the PANI-CND CE was comparable to that of the Pt CE due to its low R_{ct}. These results of CV and EIS show good consistency, and directly affect the power conversion efficiencies (PCEs) of DSSCs made with the various CE materials.

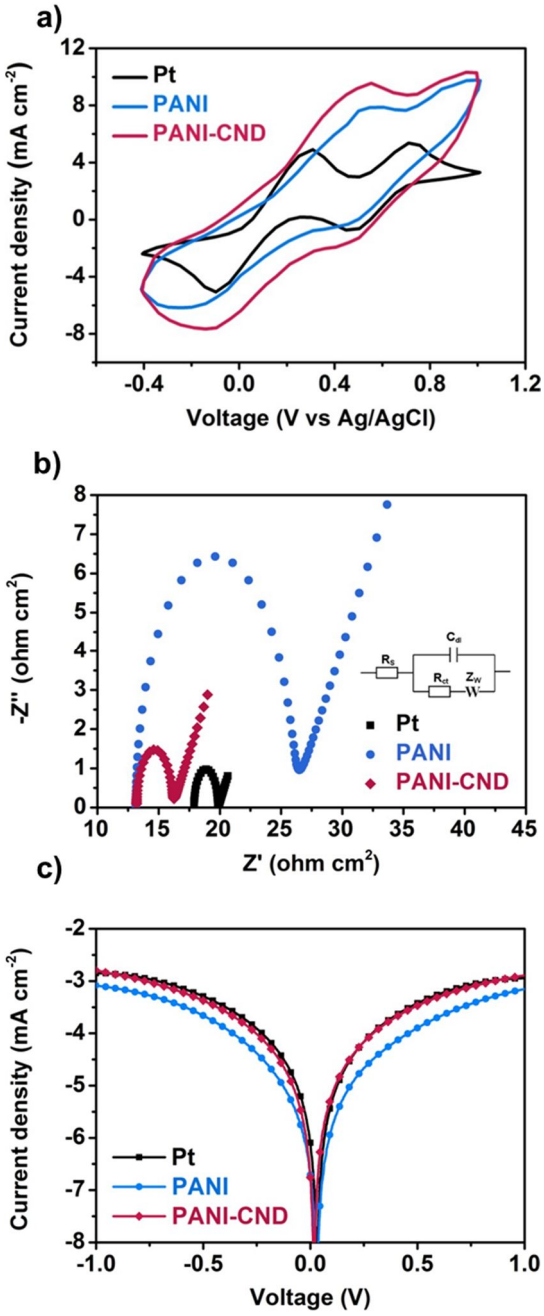
a)
Pt
PANI
PANI-CND
Current density (mA cm-2)
Voltage (V vs Ag/AgCl)
b)
-Z'' (ohm cm2)
Z' (ohm cm2)
Pt
PANI
PANI-CND
c)
Current density (mA cm-2)
Voltage (V)
Pt
PANI
PANI-CND

Figure 9. (a) CV curves of Pt, PANI and PANI-CND on FTO substrates in I^{3-}/I^{-} electrolyte composed of 10 mM LiI, 1 mM I_2, and 0.1 M $LiClO_4$ in acetonitrile at a scan rate of 50 mV s^{-1}. (b) Nyquist plots of symmetrical dummy cells employing Pt, PANI and PANI-CND counter electrodes (CEs). The frequency scan range was set from 0.1 Hz to 1 MHz with amplitude of 10 mV. Inset is the equivalent circuit. (c) Tafel polarization curves measured for the same devices used in the EIS measurements at a scan rate of 50 mV s^{-1}. PANI-CND CE for the measurements was fabricated with PANI-CND (5 wt%).

Table 2. Parameters of symmetrical dummy cells employing various counter electrodes (CEs).

Sample	R_s (Ω cm^2)	R_{ct} (Ω cm^2)
Pt	17.9	1.95
Pristine PANI	13.1	12.77
PANI-CND	13.2	2.93

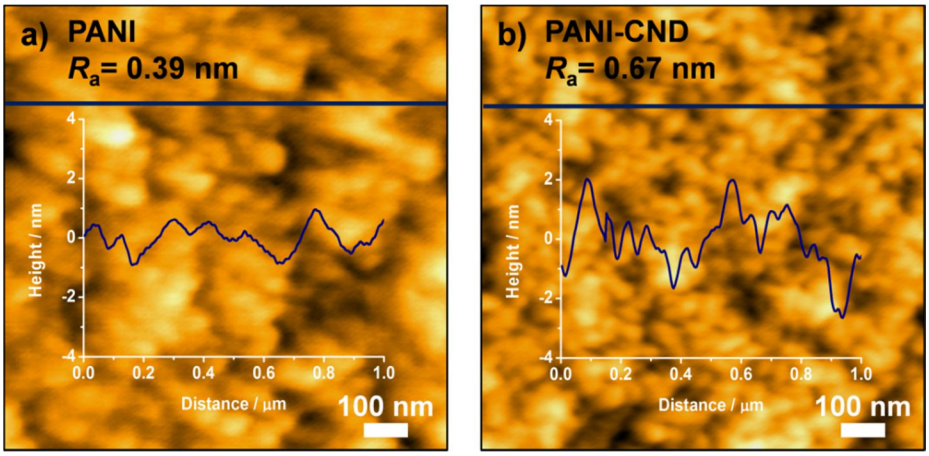

Figure 10. AFM images and cross-sectional analyses (1 X 1 μm^2 scale) of (a) PANI and (b) PANI-CND counter electrodes (CEs). Measured surface roughness (R_a) values of the samples are 0.39 and 0.67 nm, respectively. PANI-CND CE was fabricated with PANI-CND (5 wt%).

3.4.2 Photovoltaic performance of DSSC with PANI-CND CE

Figure 11 shows the *J–V* characteristics of DSSCs employing Pt, PANI, and PANI-CND CEs; the photovoltaic parameters are listed in Table 3. The photovoltaic performance data of DSSCs using PANI-CND CEs with other CND concentrations is presented in Figure 12 and Table 4. The short-circuit current density (J_{sc}) of the cells with PANI-CND CEs (13.8 mA cm^{-2}) was higher than those with Pt (13.2 mA cm^{-2}) and PANI CEs (10.1 mA cm^{-2}), indicating that more current can be collected at the PANI-CND CE, which suggests that CND nucleation consequently has a strong effect on the electro-catalytic activity of PANI [38]. The PCEs of DSSCs containing PANI-CND CEs was 7.45%, which is higher than that obtained with Pt (7.37%) or PANI (5.60%) CEs. Despite the slightly higher R_{ct} of the PANI-CND CE relative to that of the Pt CE, the lower R_s of PANI-CND CE produced good photovoltaic characteristics of DSSCs by compensating the gap in R_{ct} [38].

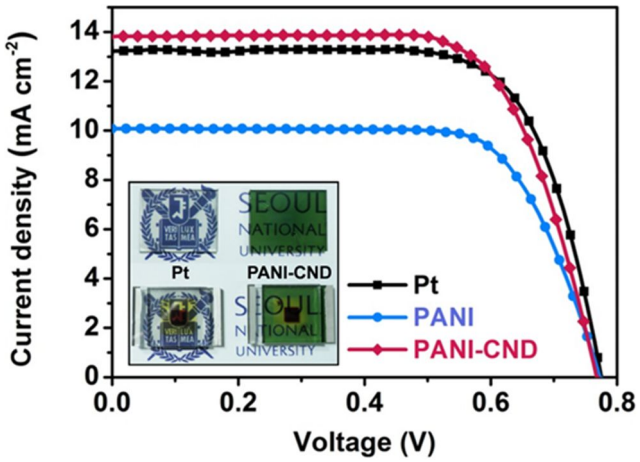

Figure 11. *J-V* characteristics of DSSCs with Pt, PANI and PANI-CND counter electrodes (CEs) and inset is a photograph of electrodes made with Pt and PANI-CND (top) and assembled DSSCs with the each CEs (bottom). PANI-CND CE for the measurements was fabricated with PANI-CND (5 wt%).

Table 3. Photovoltaic parameters of DSSCs employing various counter electrodes.

Sample	V_{oc} (V)	J_{sc} (mA cm^{-2})	*FF*	η (%)
Pt	0.78	13.2	0.72	7.37
Pristine PANI	0.77	10.1	0.72	5.60
PANI-CND	0.77	13.8	0.70	7.45

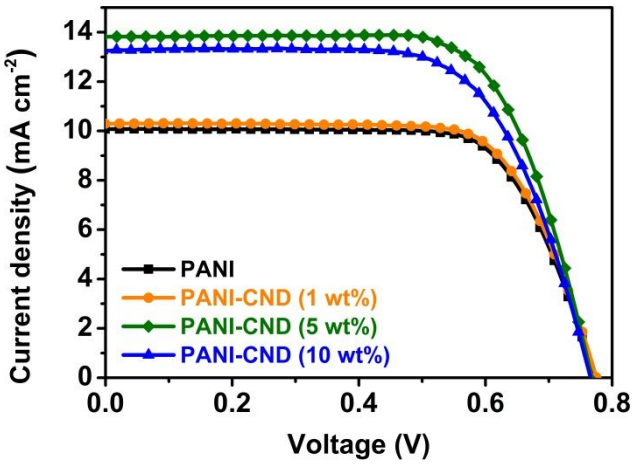

Figure 12. *J-V* characteristics of DSSCs employing PANI and PANI-C ND counter electrodes with different CNDs concentrations: 1, 5, and 1 0 wt%.

Table 4. Photovoltaic parameters of DSSCs employing PANI and PANI-CND counter electrodes with different CNDs concentrations: 1, 5, and 10 wt%.

Sample	V_{oc} (V)	J_{sc} (mA cm^{-2})	*FF*	η (%)
Pristine PANI	0.77	10.1	0.72	5.60
PANI-CND (1 wt%)	0.78	10.3	0.72	5.71
PANI-CND (5 wt%)	0.77	13.8	0.70	7.45
PANI-CND (10 wt%)	0.76	13.3	0.67	6.84

Chapter 4. Conclusion

In summary, PANI with high surface area and purity were synthesized *via* CND-induced nucleation during PANI polymerization. In the polymerization reactions, the CNDs induced homogeneous nucleation and head-to-tail coupling of aniline dimers. As a result, PANI-CND exhibited a more than 3.5 times larger surface area (43.6 $m^2 g^{-1}$) than pristine PANI (12.4 $m^2 g^{-1}$), and produced the highly conductive films (electrical conductivity: 774 S cm^{-1}) with an increased surface roughness. PANI-CND films were successfully utilized as CEs in DSSCs, exhibiting a higher conversion efficiencies (η= 7.45%) than those of both the conventional Pt CEs (η= 7.37%) and the CEs made with pristine PANI (η= 5.60%). The procedures detailed herein provide an efficient and facile means of producing high-performance PANI electrodes for DSSCs or other applications.

References

[1] S. Thomas, T. G. Deepak, G. S. Anjusree, T. A. Arun, S. V. Nair and A. S. Nair, *J. Mater. Chem. A*, **2014**, *2*, 4474-4490.

[2] H. Wang and Y. H. Hu, *Energy Environ. Sci.*, **2012**, *5*, 8182.

[3] S. Yun, A. Hagfeldt and T. Ma, *Adv. Mater.*, **2014**, *26*, 6210.

[4] B. Anothumakkool, O. Game, S. N. Bhange, T. Kumari, S. B. Ogale and S. Kurungot, *Nanoscale*, **2014**, *6*, 10332.

[5] S. S. Jeon, C. Kim, J. Ko and S. S. Im, *J. Mater. Chem.*, **2011**, *21*, 8146.

[6] Y. Xiao, G. Han, Y. Li, M. Li and Y. Chang, *J. Mater. Chem. A*, **2014**, *2*, 3452.

[7] B. He, Q. Tang, T. Liang and Q. Li, *J. Mater. Chem. A*, **2014**, *2*, 3119.

[8] Q. Tai, B. Chen, F. Guo, S. Xu, H. Hu, B. Sebo and X.-Z. Zhao, *ACS Nano*, **2011**, *5*, 3795.

[9] J. S. Lee, M. Kim, J. Oh, J. Kim, S. Cho, J. Jun and J. Jang, *J. Mater. Chem. A*, **2015**, *3*, 7029.

[10] S. Cho, K.-H. Shin and J. Jang, *ACS Appl. Mater. Interfaces*, **2013**, *5*, 9186.

[11] K.-Y. Shin, M. Kim, J. S. Lee and J. Jang, *Sci. Rep.*, **2015**, *5*, 13615.

[12] S. H. Park, K.-H. Shin, J.-Y. Kim, S. J. Yoo, K. J. Lee, J. Shin, J. W. Choi, J. Jang and Y.-E. Sung, *J. Photochem. Photobiol. A*, **2012**, *245*, 1.

[13] S. Cho, S. H. Hwang, C. Kim and J. Jang, *J. Mater. Chem.*, **2012**, *22*,

12164.

[14] S. S. Jeon, C. Kim, T. H. Lee, Y. W. Lee, K. Do, J. Ko and S. S. Im, *J. Phys. Chem. C*, **2012**, *116*, 22743.

[15] S. H. Lee, D. H. Lee, K. Lee and C. W. Lee, *Adv. Funct. Mater.*, **2005**, *15*, 1495.

[16] D. Li, J. Huang and R. B. Kaner, *Acc. Chem. Res.*, **2008**, *42*, 135.

[17] S. Y. Lim, W. Shen and Z. Gao, *Chem. Soc. Rev.*, **2015**, *44*, 362.

[18] Y. Dong, J. Shao, C. Chen, H. Li, R. Wang, Y. Chi, X. Lin and G. Chen, *Carbon*, **2012**, *50*, 4738.

[19] X. T. Zheng, A. Ananthanarayanan, K. Q. Luo and P. Chen, *Small*, **2015**, *11*, 1620.

[20] W. Kwon, G. Lee, S. Do, T. Joo and S.-W. Rhee, *Small*, **2014**, *10*, 506.

[21] D. Qu, M. Zheng, L. Zhang, H. Zhao, Z. Xie, X. Jing, R. E. Haddad, H. Fan and Z. Sun, *Sci. Rep.*, **2014**, *4*, 5294.

[22] P. Tang, *Org. Synth.*, **2005**, *81*, 262.

[23] V. R. Pattabiraman and J. W. Bode, *Nature*, **2011**, *480*, 471.

[24] C. M. Luk, B. L. Chen, K. S. Teng, L. B. Tang and S. P. Lau, *J. Mater. Chem. C*, **2014**, *2*, 4526.

[25] E. Hwang, S. Seo, S. Bak, H. Lee, M. Min and H. Lee, *Adv. Mater.*, **2014**, *26*, 5129.

[26] J. Lee, S. H. Hwang, J. Yun and J. Jang, *ACS Appl. Mater. Interfaces*, **2014**, *6*, 15420.

[27] C. M. Yoon, S. Lee, S. H. Hong and J. Jang, *J. Colloid Interface Sci.*, **2015**, *438*, 14.

[28] J. Yun, S. H. Hwang and J. Jang, *ACS Appl. Mater. Interfaces*, **2015**, *7*, 2055.

[29] M. Kim, S. Cho, J. Song, S. Son and J. Jang, *ACS Appl. Mater. Interfaces*, **2012**, *4*, 4603.

[30] N. Gospodinova and L. Terlemezyan, *Prog. Polym. Sci.*, **1998**, *23*, 1443.

[31] Y. Wei, R. Hariharan and S. A. Patel, *Macromolecules*, **1990**, *23*, 758.

[32] M. Kim, C. Lee and J. Jang, *Adv. Funct. Mater.*, **2014**, *24*, 2489.

[33] K. Lee, S. Cho, S. Heum Park, A. J. Heeger, C.-W. Lee and S.-H. Lee, *Nature*, **2006**, *441*, 65.

[34] B. H. Lee, S. H. Park, H. Back and K. Lee, *Adv. Funct. Mater.*, **2011**, *21*, 487.

[35] C. L. Wang, J. Y. Liao, S. H. Chung and A. Manthiram, *Adv. Energy Mater.*, **2015**, *5*, 1401524.

[36] P. Zhai, T. C. Wei, Y. H. Chang, Y. T. Huang, W. T. Yeh, H. Su and S. P. Feng, *Small*, **2014**, *10*, 3347.

[37] N. Papageorgiou, *Coord. Chem. Rev.*, **2004**, *248*, 1421.

[38] E. Bi, H. Chen, X. Yang, W. Peng, M. Grätzel and L. Han, *Energy Environ. Sci.*, **2014**, *7*, 2637.

[39] J. Wu, Y. Li, Q. Tang, G. Yue, J. Lin, M. Huang and L. Meng, *Sci. Rep.*, **2014**, *4*, 4028.

[40] Y. C. Wang, D. Y. Wang, Y. T. Jiang, H. A. Chen, C. C. Chen, K. C. Ho, H. L. Chou and C. W. Chen, *Angew Chem., Int. Ed.*, **2013**, *52*, 6694.

초 록

본 실험에서는 탄소 나노점을 기핵제로 사용하여 다공성 나노구조를 지닌 폴리아닐린을 제조하고, 이를 염료감응형 태양전지의 상대전극으로 활용하였다. 아닐린 단량체와 결합된 탄소 나노점은 중합 반응의 핵으로서 효율적으로 작용하였다. 탄소 나노점은 고분자가 뭉친 구조로 이어질 수 있는 2차 성장 반응을 억제하였고, 표면적이 큰 다공성의 폴리아닐린을 형성할 수 있도록 하였다 (총 표면적: 43.6 m^2g^{-1}). 또한, 중합 용액에서 탄소 나노점은 헤드-투-테일 2량체 생성을 촉진하여 폴리아닐린의 분자구조 내 파라방향 결합도를 높였다. 이러한 탄소나노점 기핵제의 효과로, 제조된 폴리아닐린-탄소 나노점 나노복합재 박막의 전기전도도가 774 S cm^{-1}까지 증가하였다. 폴리아닐린-탄소 나노점 나노복합재 박막을 염료감응형 태양전지의 상대전극으로 활용하였으며, 기존의 백금 상대전극 (η= 7.37%)과 폴리아닐린 상대전극 (η= 5.60%)을 사용하였을 때보다 높은 7.45%의 전력변환효율을 얻을 수 있었다. 이 논문은 염료감응형 태양전지나 여타 다른 소자를 위한 고성능의 폴리아닐린 전극을 제조하는 효율적이며 간단한 방법을 제공하는데 목적이 있다.

주요어 : 폴리아닐린, 탄소 나노점, 자체 분산 중합, 염료감응형 태양전지, 상대전극.

학번 : 2014-20627